STUDIA UBB CHEMIA, LXXI, 2, 2026 (p. 243-263)
(RECOMMENDED CITATION)
DOI:10.24193/subbchem.2026.2.13

VISUALIZATION OF LATENT FINGERPRINTS BY COMBINED TETRA-*N*-BUTYLAMMONIUM IODIDE DUSTING AND NITROGEN DIOXIDE TREATMENT: MECHANISTIC INSIGHTS

Varinder SINGH[a], Metodija NAJDOSKI[b], Om Prakash JASUJA[a], Slobodan OKLEVSKI[c], Sasho STOJKOVIKJ[d,*]

ABSTRACT. The development of methods for latent fingerprints visualization is still attractive considering that there is no approach that is universal for all types of fingerprints and substrates. A thorough understanding of the visualization mechanism is crucial for expanding methods application and making them practical for real case scenarios. In this research, nitrogen dioxide (NO_2) treatment, previously limited to thermal paper substrates, is expanded towards visualization of latent fingerprints on various non-porous and porous substrates by introduction of pre-treatment with tetra-*n*-butylammonium iodide (TBAI). The visualization processes were studied using Raman, UV-Visible, FTIR and ^{1}H NMR spectroscopy, combined with various validation experiments. The results show that formation of molecular iodine (I_2), generated by reactions between NO_2 and TBAI, plays a key role in the visualization mechanism. The as-generated I_2 further reacts with excess TBAI, producing tetra-*n*-butylammonium triiodide ($TBAI_3$). $TBAI_3$ is a dark colored compound that provides the dominating contrast of the visualized fingerprint. Besides reactant, TBAI resembles a role of a phase-transfer catalyst that enables NO_2 to penetrate deeper into fingerprint's residue and to react with the fatty acid esters producing intrinsically colored nitro-compounds that additionally contribute towards fingerprints visualization effect.

Keywords: *Latent fingerprints visualization, Tetra-n-butylammonium iodide, Nitrogen dioxide*

[a] *RIMT University, Punjab, India.*
[b] *Institute of Chemistry, Faculty of Natural Sciences and Mathematics, Ss. Cyril and Methodius University - Skopje, Arhimedova 5, 1000, Skopje, Republic of North Macedonia.*
[c] *Ministry of Interior, Republic of North Macedonia.*
[d] *MIT University Skopje, Boris Trajkovski 62, 1000 Skopje, Republic of North Macedonia.*
* *Corresponding author: sasho.stojkovikj@dm.mit.edu.mk*

©2026 STUDIA UBB CHEMIA. Published by Babeş-Bolyai University.
This work is licensed under a Creative Commons Attribution-NonCommercial-NoDerivatives 4.0 International License.

INTRODUCTION

Latent fingerprint visualization has long served as an essential aspect of forensic identification due to the uniqueness and persistence of friction ridge patterns. Various traditional methods such as dusting, ninhydrin treatment, cyanoacrylate fuming etc. have been widely used to visualize latent prints on variety of surfaces in terms of composition and surface morphology. These techniques often offer good efficacy, yet in many cases they suffer from limitations related to substrate specificity or destructive nature of the process during the print development. For example, ninhydrin/solvent-based reagents can have issues related to the solvent itself. Namely, if a paper on which fingerprints are to be developed has ink writings, the ink may bleed in contact with the solvent used for preparation of the ninhydrin solutions [1] hence important evidence might be lost. To address such problems, many researchers have looked for an alternative method where either modified application method is used [2] or intermediate and alternative solvents are used to apply the ninhydrin [3]. Researchers reported visualization based on UV light induced luminescence of latent fingerprints after treating the sample with electric discharge in nitrogen gas and subsequent exposure to vapors formed by heating ammonium hydrogen carbonate [4]. Recent research appeared in literature where efforts have been made to develop latent fingerprints with solvent- free chemicals. Kelly et al. [5] reported the use of sulfur nitrides and Shah [6] used selenium dioxide, phosphorus sulfides and hexachlorophosphazene in vapor phase to develop latent fingerprints on various surfaces. Clarke et al. [7] reviewed the status of solvent free methods to visualize latent fingerprints and claims that dry transfer method for porous surfaces was found to be most promising among all existing solvent-free methods. Regarding the solvent-free, among physical and chemical methods, iodine fuming, as one of the oldest methods, is safe and non-destructive visualization approach, suitable for both aged and freshly impressed latent prints on porous and semi-porous surfaces [8]. However, the temporary nature of iodine-developed prints due to iodine sublimation and lack of fixation has posed a significant challenge to its long-term forensic application. Researchers have attempted to stabilize iodine-developed prints using starch, paraffin wax, or post-treatment with chemical fixatives, but these often introduce complications such as color interference or surface alteration [9-10]. The fingerprint development methods can be significantly improved if the visualization mechanism is well understood. The spectroscopic characterization techniques such as Raman and FTIR can play a pivotal role [11-12]. Namely, in one of our previous studies, tetra-*n*-butylammonium iodide - $(C_4H_9)_4NI$ (abbreviated as TBAI), a quaternary ammonium salt with phase-transfer catalytic (PTC) properties, was used for

sample dusting prior to iodine fuming thus achieving successful and irreversible iodine fixation and the chemical reaction mechanism during the course of fingerprint development was characterized using FTIR, Raman and UV–Visible spectroscopy [11]. Another previous study was focused on developing latent fingerprints using nitrogen dioxide (NO_2) treatment [13]. However, the NO_2 method is only limited to visualization of latent fingerprints on thermal paper samples and showed poor performance when visualizing prints impressed on other materials. Introducing TBAI powdering and subsequent NO_2 gas treatment expands both the application of the NO_2 method [13] and further application of the phase-transfer catalyst TBAI, that was successfully combined with the iodine fumes treatment [11]. The overall evaluation of the visualization performance from such combination of both methods (abbreviated as TBAI/NO_2 method in the following text) and the possibility to visualize fingerprints on various substrate types, showed valuable results, simplicity of the method and perspective for its application in forensic scenarios. This opened an opportunity for deeper understanding of the chemical background leading to fingerprint visualization effects, thus studying the reaction mechanisms represents the main focus of this research. For that purpose, we utilized several spectroscopic characterization techniques in combination with various validation experiments.

RESULTS AND DISCUSSION

Forensic evaluation of the TBAI/NO_2 method

The forensic examination of visualized fingerprints impressed on various substrate types significantly highlights how surface characteristics apply on the quality and clarity of papillary ridge detail, which is crucial for identification purposes. Therefore, the fingerprints visualization capacity of the TBAI/NO_2 method proposed in this research is evaluated on sebaceous latent fingerprints impressed on various porous and non-porous surfaces such as standard office paper, laminated wooden chipboard, glass and glazed ceramics. The as-visualized fingerprints are presented in Figure 1, while the results from qualitative and quantitative evaluation of the method, in Table 1 and Table 2, respectively.

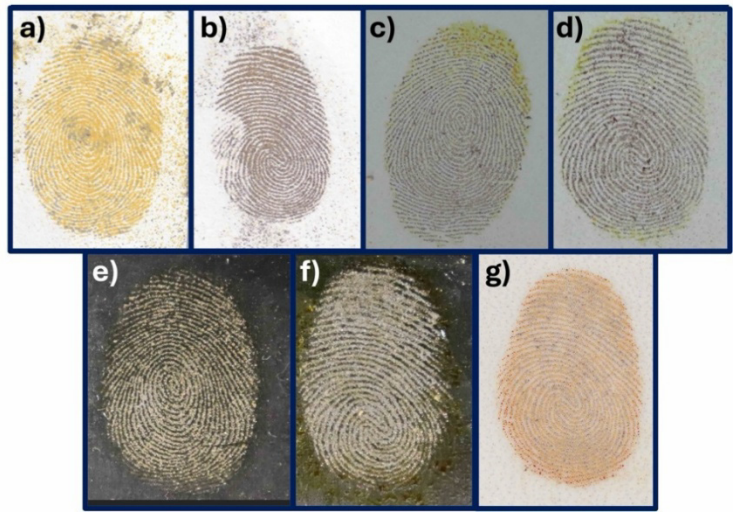

Figure 1. Visualized sebaceous fingerprints on various porous and non-porous surfaces: **(a, b)** Standard 80 gsm paper; **(c, d)** Laminated chipboard; **(e, f)** Glass and **(g)** Glazed ceramic.

Table 1. Comparative qualitative analysis of latent fingerprints visualized on various types of substrates, presented in Figure 1.

Substrate type	Surface	Pattern type	Ridge clarity
(a) Standard 80 gsm paper – Fingerprint 1	Porous	Whorl	Good
(b) Standard 80 gsm paper – Fingerprint 2	Porous	Whorl	Good
(c) Laminated chipboard – Fingerprint 1	Non-porous, smooth	Whorl	Excellent
(d) Laminated chipboard – Fingerprint 2	Non-porous, smooth	Whorl	Excellent
(e) Glass – Fingerprint 1	Non-porous, smooth	Whorl	Excellent
(f) Glass – Fingerprint 2	Non-porous, smooth	Whorl	Moderate
(g) Glazed ceramic	Non-porous, glazed	Whorl	Good

Table 2. Identification of 2nd level minutiae and 3rd level features and evaluation of the forensic suitability for the latent fingerprints visualized on various types of substrates, presented in Figure 1.

Substrate type	2nd level minutiae	3rd level features visibility	Forensic suitability
(a) Standard 80 gsm paper – Fingerprint 1	50	Not visible	High
(b) Standard 80 gsm paper – Fingerprint 2	45	Not visible	Moderate
(c) Laminated chipboard – Fingerprint 1	59	Partially visible	High
(d) Laminated chipboard – Fingerprint 2	59	Partially visible	High
(e) Glass – Fingerprint 1	45	Partially visible	High
(f) Glass – Fingerprint 2	30	Not visible	Moderate
(g) Glazed ceramic	41	Not visible	Sufficient

Porous substrates, such as standard office paper, generally enable visualization of continuous ridge patterns with acceptable contrast. However, the partially absorbent nature of the substrate prevents the clear manifestation of 3rd level features, such as ridge edge contours and pore structures. Despite this limitation, the quantification of 45–50 identifiable 2nd level minutiae ensure the possibility of conducting reliable comparative analyses, consistent with the international forensic guidelines [14-15].

On the other hand, surfaces with non-porous and smooth finish, such as laminated chipboards, provide highly suitable conditions for detection and visualization of latent fingerprints. These materials enable formation of outlined ridge patterns with very significant contrast versus the background surface. Therefore, the TBAI/NO_2 method provides extensive number of 2nd level features (up to 59 minutiae), also observing 3rd level details, including pores and edge features. Glazed ceramic materials, due to their smoothness enable satisfactory development of papillary ridge patterns, ensuring clear separation between ridges and furrow spaces. In the examined cases, up to 41 – 2nd level minutiae are identified, much higher than the thresholds for comparative purposes [14-15]. Nevertheless, 3rd level features cannot be identified. Finally, glass surfaces which encompass very smooth texture offer favorable conditions for latent fingerprint visualization. Hence, the visualized fingerprints exhibit strong contrast and clear ridge contours, leading to quantification of up to 45 – 2nd level minutiae, again higher than the reported minutiae thresholds [14-15]. Partial visibility of 3rd level features is further enhancing the value of the TBAI/NO_2 method for forensic applications in real case scenarios.

In summary, the TBAI/NO_2 method is simple, fast, reliable and practical for utilization in forensic laboratories. The forensic evaluation shows that smooth and non-porous surfaces offer optimal conditions for detecting 2nd level fingerprint features and, in certain areas, elements of 3rd level detail, collectively enhance the reliability of forensic identification, while the porous substrates enable identification processes that rely predominantly on 2nd level fingerprint features.

Furthermore, it is obvious from the images on Figure 1 that the color of the visualized fingerprints can differ even when impressed on the same type of substrate, especially noticeable in the case of the fingerprints impressed on paper's surface i.e., the fingerprint on Figure 1a is mostly orange in color, while the one on Figure 1b is brown when visualized via the TBAI/NO_2 method. The fingerprints impressed on laminated chipboard are predominately brownish, but significant orange color area can be observed on Figure 1c. This could possibly imply to differences in the visualization mechanism related to the chemical processes between TBAI, NO_2 and fingerprint's sebaceous residue, which is found to be worth studying in the scope of this research.

Study of fingerprint visualization mechanism

Characterization with Raman spectroscopy

The characterization started with Raman spectroscopy analysis of the fingerprints impressed on glass as non-porous and paper as porous substrate, visualized under 5- and 20 s exposures to NO_2, after being dusted with TBAI. The sample preparation procedures are given in Table S1 in SI and the Raman spectra results are presented in Figure 2a and Figure S1 in SI (full range Raman spectra).

The Raman spectra of the fingerprints impressed on glass and paper surfaces, exposed to NO_2 for 5 s show features that are typical for vibrational modes in I_3^- ion [16-17]: strong band attributed to symmetric stretching vibration at ~112 cm^{-1} with a shoulder at ~145 cm^{-1}, that can be recognized as asymmetric stretching vibration. This is suggesting that the visualization mechanism follows identical pathways, as presented in our previous research [11], that is formation of tetra-*n*-butylammonium triiodide - $TBAI_3$, according to Eq. 1. Moreover, the visualized fingerprints with 5 s NO_2 treatment appear very similar in color - dark yellow on both glass and paper surfaces, as described in Table S1 in SI, albeit pure $TBAI_3$ is a very dark-colored compound [11].

$$TBAI + I_2 \rightarrow TBAI_3 \qquad \text{Equation 1}$$

The second set of spectra in Figure 2a are recorded on fingerprints impressed on paper surfaces, from which one is immediately visualized, and one was visualized 2 months prior to characterization, both with 20 seconds NO_2 treatment. The immediately visualized fingerprint appeared orange in color, while the one developed after 2 months - dark brown (Table S1 in SI). Besides the distinctive bands characteristic for the fundamental vibrational modes of the I_3^- anion [11, 16-17] at ~112 and ~110 cm^{-1} for the immediately visualized- and the fingerprint visualized after 2 months, respectively, additional distinctive bands can be observed at higher wavenumbers for both samples. Namely, one band appears at ~167 cm^{-1} with a small shoulder at ~148 cm^{-1} in the case of the immediately visualized fingerprint, whilst a strong band is observable at ~220 cm^{-1} for the fingerprint visualized 2 months prior to the characterization with Raman spectroscopy. According to some literature data [18-19], the band at ~167 cm^{-1} including the shoulder at ~148 cm^{-1}, observable in the spectrum of the immediately visualized fingerprint, could be attributed to vibrations in polyiodide ions [18] and vibrations in perturbed I_2 molecule together with symmetric/asymmetric vibrations in the I_3^- anion [19]. The band at ~220 cm^{-1} in the spectrum of the fingerprint visualized 2 months prior to

the characterization could possibly be attributed to overtone of the fundamental bending vibration in the I_3^- ion [17] appearing at ~110 cm^{-1}. However, the absence of such distinctive overtone bands in the spectra of the other visualized fingerprints on glass and paper remains an open question. A very weak feature is observable at ~1100 cm^{-1} in the spectrum of immediately visualized fingerprint on paper with 20 s NO_2 treatment which can be possibly attributed to aliphatic stretching vibrations in the butyl groups [11, 20]. Additional very weak features can be observed in the Raman spectra of the visualized fingerprints in Figure 2 and Figure S1 in SI (full range Raman spectra), yet their interpretation can be neglected at this point. The identification of I_3^- anion in the fingerprint that is characterized 2 months after being visualized, shows that the as formed $TBAI_3$ remains stable and no additional post-treatment or fixation is required. This is very suitable for preservation of important forensic evidence.

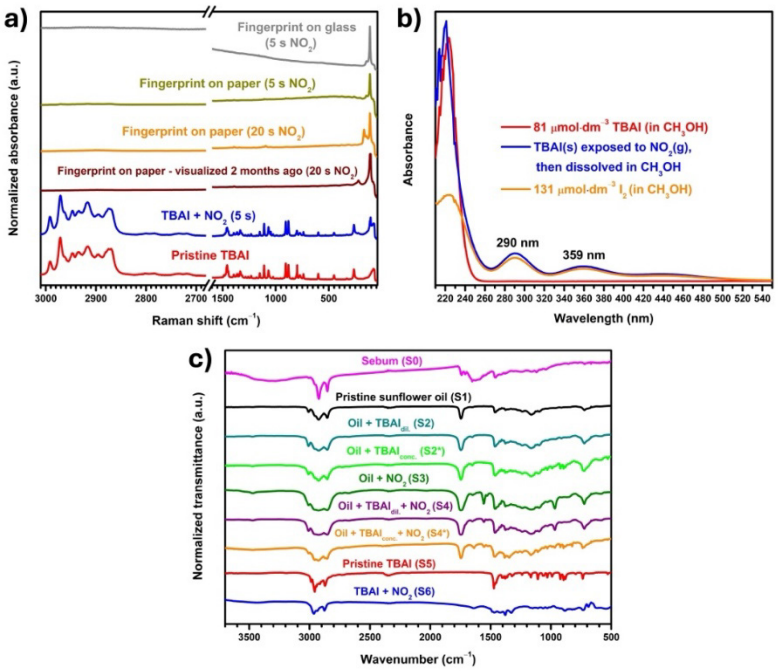

Figure 2. (a) Raman spectra of visualized fingerprints on glass and paper surfaces under various conditions and Raman spectra of pristine TBAI and TBAI treated with NO_2 gas: **(b)** UV-Vis spectra of TBAI, TBAI exposed to NO_2 and of iodine, recorded in methanol as solvent; **(c)** FTIR spectra of various samples including human sebum residue (Sample 0), pristine sunflower oil (Sample 1), sunflower oil treated under different conditions (Sample 2–Sample 4*), pristine TBAI as a reference material (Sample 5) and TBAI exposed to NO_2 (Sample 6).

Up to now it is quite certain that the latent fingerprint coloration mechanism is most possibly based on the formation of $TBAI_3$ via reaction between TBAI and I_2 (Eq. 1), as in the case of our previous research [11], and according to the previous discussion, even polyiodide ions [18] can be formed. Nevertheless, the question that arises at this point is what is the origin of the molecular iodine that reacts with TBAI? In order to tackle this question, Raman spectra are recorded on pristine TBAI and TBAI exposed to NO_2 gas for 5 seconds. The sample preparation is described in Table S1 in SI. According to the results presented in Figure 2 and Figure S1 in SI (full range Raman spectra), the NO_2 treated TBAI resembles all spectral features as in the case of pristine TBAI with an exception in the region below 200 cm^{-1}. The bands typical from C–C and C–H stretching and C–H bending vibrational modes can be typically assigned in the region 3000–1000 cm^{-1} region [11, 20-21], originating from the four n-butyl groups. Moreover, the region between 1000 and 300 cm^{-1}, is typical for various vibrations involving the $–CH_2–$, $–CH_3$ groups, C–C skeleton and C–N bonds in the case of TBA^+ cation [21], but also for other aliphatic quaternary ammonium compounds [22], while the bands at ~262 cm^{-1} in both spectra are possibly related to TBA^+ cation lattice vibrations and the position of this band is influenced by the anion's chemical identity and presence of crystalline water [11, 20, 23]. Similar anion-cation interaction affected modes in the TBA^+ group are the most probable reason for observation of the broad feature at ~75 cm^{-1}. Though, a band at ~108 cm^{-1} is clearly visible only in the spectrum of NO_2 treated TBAI, which also appears in the spectra of all visualized fingerprints on various surfaces, and which is assigned to fundamental vibrational modes of the I_3^- anion [11, 16-17], as discussed in the text above. This is suggesting that few seconds of NO_2 exposure is transforming TBAI into $TBAI_3$ via oxidation of the I^- anion into molecular I_2. Subsequently, I_2 reacts with excess TBAI to form $TBAI_3$, as described with Eq. 1. Regarding the oxidation of the I^- anion with gaseous NO_2, there are several possible reactions (Eq. 2–7), from which some are reported in the literature [24]. Eq. 2 represents the simplest case describing net oxidation of I^- anion directly with NO_2. The gaseous NO_2 can also dimerize and establish an equilibrium with N_2O_4, according to Eq. 3, whereas N_2O_4 is reported to be more reactive than NO_2, thus oxidizing the I^- anion into molecular I_2 [24] according to Eq. 4.

$$2I^- + 2NO_2 \rightarrow I_2 + 2NO_2^- \qquad \text{Equation 2}$$

$$2NO_2 \rightleftarrows N_2O_4 \qquad \text{Equation 3}$$

$$2I^- + N_2O_4 \rightarrow I_2 + 2NO_2^- \qquad \text{Equation 4}$$

However, the presence of moisture (water vapor) in the reaction vessel for treating the latent fingerprints with NO_2, based on exothermic reaction between Zn and HNO_3 [13], cannot be neglected. The water vapor

can react with both NO_2 and N_2O_4 and form HNO_3 and HNO_2 according to Eq. 5 and 6, respectively.

$$2NO_2 + H_2O \rightarrow HNO_3 + HNO_2 \quad \text{Equation 5}$$
$$N_2O_4 + H_2O \rightarrow HNO_3 + HNO_2 \quad \text{Equation 6}$$

HNO_3 can subsequently oxidize the I^- anion into molecular I_2, according to Eq. 7:

$$6I^- + 8H^+ + 2NO_3^- \rightarrow 3I_2 + 2NO + 4H_2O \quad \text{Equation 7}$$

Other side reactions between the I^- anion, NO_2 and their products are also possible to occur, yet the main point of this discussion is that when nitrogen resembles oxidation states of +4 and +5, such compounds are strong oxidizers that can easily transform the I^- anion into I_2 which can further react with excess TBAI to form the colored compound $TBAI_3$ (Eq. 1), achieving visualization of the latent fingerprints.

Characterization with UV-Vis spectroscopy

To further clarify that molecular I_2 is formed via oxidation of the I^- anion when exposed to NO_2, pristine TBAI, TBAI exposed to NO_2 for 5 seconds and pristine I_2 crystals are dissolved in polar organic solvents and characterized with UV-Visible spectroscopy. The first attempt was to use *tert*-butanol as a solvent for this purpose, yet however it was observed that when pristine TBAI is dissolved in this solvent in various concentrations, the UV-Vis spectra show identical absorption maximums, as in the case of TBAI exposed to NO_2 (Figure S3 in SI), and moreover the solution turned pale yellow in color suggesting per se formation of molecular I_2 from TBAI (Figure S4 in SI). Nonetheless, the main discussion of this phenomenon and its possible explanations are presented in Subsection S2.2 in SI. Therefore, another attempt was made, and methanol was used as a solvent instead, as in the case of our previous research [11]. The preparations of the samples for characterization with UV-Vis spectroscopy are presented in Table S2 in SI and the recorded spectra in Figure 2b. The spectrum of TBAI in CH_3OH shows distinctive absorption only in the UV region with sharp peak at ~227 nm. When TBAI is exposed to NO_2 for 5 minutes and dissolved in CH_3OH, besides the absorption in the UV region that shifts towards lower wavelength (~221 nm), two more broad peaks at 290 and 359 nm, appear. These results are in agreement with the UV-Vis spectra of TBAI and $TBAI_3$ in our previous publication [11], and they are generally attributed to absorption from I_3^- anion [25-26]. Furthermore, the broad peaks at 290 and 359 nm are also observable in the spectrum of I_2 in CH_3OH. This is suggesting that these

peaks are likely not originating only from a single specie but rather from several species in equilibrium. Namely, the $TBAI_3$ formed when TBAI is exposed to NO_2 (via the molecular I_2 mechanism discussed above) undergo dissociation in the solution according to Eq. 8.

$$TBAI_3\,(solution) \rightarrow TBA^+\,(solution) + I_3^-\,(solution) \qquad \text{Equation 8}$$

The I_3^- forms an equilibrium with the I^- anion and molecular I_2, according to Eq. 9, which is the reason for the characteristic peaks (at 290 and 359 nm) overlapping in the UV-Vis spectra of both I_2 and TBAI exposed to NO_2 (Figure 2b).

$$I_3^-\,(solution) \rightleftarrows I^-\,(solution) + I_2\,(solution) \qquad \text{Equation 9}$$

The results from the UV-Vis- strongly support the Raman spectroscopy findings and from both discussions can be concluded that molecular I_2 is indeed formed via oxidation of the I^- anion from TBAI, subsequently reacting with excess TBAI to form $TBAI_3$ (Eq. 1), achieving visualization of the latent fingerprints.

Regarding the utilization of *tert*-butanol as solvent for characterization with UV-Vis spectroscopy, the UV-Vis spectrum of pristine TBAI dissolved in this solvent shows the characteristic peaks at 292 and 360 nm that can be attributed to the $I_3^-/I^-/I_2$ equilibrium (Figure S2 in SI) and the solution turns pale yellow (Figure S3 in SI) over the course of few hours regardless whether the solution is kept in dark or exposed to sunlight. This means that the I^- anion from TBAI is undergoing per se oxidation into I^- when dissolved in tert-butanol but the actual reason for such behavior is not very clear, though the possibility of photochemical processes is excluded. Subsection S2.2 in SI is dedicated to discussion of such empirical observations.

The fingerprints visualization mechanism appears to be rather clear when exclusively interactions between TBAI and NO_2 leading to formation of the colored compound $TBAI_3$ are observed, and the key process in the pathways is the formation of I_2 via oxidation of the I^- anion from TBAI. The question that subsequently follows up is: What is the role of the sebaceous residue from which latent fingerprints are composed of, in the overall visualization process? Observing all Raman spectra presented in Figure 2a, bands associated to vibrations typical for lipidic compounds that are present in the human sebum from which fingerprints are naturally composed of, are not identified. Furthermore, utilizing Raman spectroscopy to probe the surface of freshly impressed latent fingerprint prior to visualization (labelled as human sebum - Sample 0 in Table S1 in SI) has somewhat expectedly led to obtaining an ill-shaped spectrum, presented in Figure S4 in the SI. The absence of distinctive features originating from lipids in the human sebum spectrum is possibly

caused by the amorphous nature of the sebaceous residue, showing that utilizing only Raman and UV-Vis spectroscopy in the available configurations that are used in this research, are not sufficient to fully resolve the visualization mechanism. Therefore, additional characterization methodologies and experimental approaches are required.

Characterization with FTIR spectroscopy

The following discussion is mainly focused on the results obtained from characterization using FTIR and ^{1}H NMR spectroscopy. Starting with FTIR spectroscopy, the general sample preparation for characterization is presented in the Supplementary Information – SI, while the specific sample preparation/abbreviations are presented in Table S4 in SI. All recorded FTIR spectra are presented in Figure 2c. The FTIR characterization of latent fingerprint, when freshly impressed on KBr tablet, is significantly more successful compared to the Raman spectroscopy, that is, the spectrum of Sample 0 indeed shows features originating from vibrations associated with various functional groups characteristic for triglycerides and fatty acids, that are typically present in the human sebum residue. Namely, the strong bands at ~2924 cm^{-1} and ~2841 cm^{-1} are attributed to the asymmetric and symmetric stretching of aliphatic C–H bonds in $–CH_2–$ groups [27]. The broad band above 3100 cm^{-1} can be attributed to O–H group stretching vibrations due to presence of moisture [27], possibly excreted from the human sweat glands. The bands at ~1746 and ~1712 cm^{-1} are attributed to C=O group stretching vibrations, originating from esters and free fatty acids, respectively [27-28]. The broad band peaking at ~1645 cm^{-1} can possibly arise from C=C stretching vibrations in unsaturated fatty acids and their esters [27], while the bands at ~1460 cm^{-1} correspond to $–CH_2–$ groups bending modes [27-28] and the weak feature at ~1120 cm^{-1} is generally attributed to stretching C–O vibrations in ester groups [27]. However, the broad band at ~1645 cm^{-1} can also be identified for H–O–H bending vibrations in water molecules [29], which together with the broad band above 3100 cm^{-1} arising from O–H group stretching vibrations are indeed identifying presence of water. Additionally, the weak band at ~712 cm^{-1} arises from rocking-bending vibrations in CH_2 groups [27], indicating the presence of hydrocarbon chains. The band at ~1745 cm^{-1} in the spectrum of Sample 0 is significantly more prominent (lower absolute transmittance) compared to the one at ~1712 cm^{-1}, suggesting that the ester forms, that is, glycerides, are rather more abundant in the human sebum compared to free fatty acids [28]. The composition of human sebum can be variable, and such variations generally originate from body part, age, diet, ethnicity, climate etc. [28,

30-31], but also from other factors such as substrate types used for impressing (deposition of) the fingerprint, timescale between deposition and analysis, deposition conditions etc. [30]. Subjecting the latent fingerprints impressed on KBr tablets to TBAI dusting and NO_2 gas treatment for the purpose of characterizing the visualized fingerprints with FTIR spectroscopy and studying the visualization mechanism is rather challenging due to the fact that bromide anion from KBr is prone to reaction with NO_2. On the other hand, the FTIR-, in the configuration utilized for this research is typically bulk sensitive compared to the Raman spectroscopy, limiting the possibility for experimenting with very small quantities of sebaceous material in terms of characterizing the products obtained from possible interactions of the human sebum with TBAI and NO_2 and moreover collecting large amount of sebaceous residue, and later treating it with TBAI and NO_2 in a laboratory vessel, was found not to be very feasible approach. Therefore, we decided to use refined cooking sunflower oil as a reasonable substitute for the human sebum residue and proceed with the experiments and characterization.

The FTIR spectrum of pristine sunflower oil (Sample 1) in Figure 2c resembles all key features as in the case of the human sebum residue including significantly higher abundance of ester forms (glycerides) compared to free fatty acids, as mentioned above, since the band at ~1745 cm^{-1}, typical for C=O stretching vibrations in ester groups [32], is clearly observable. Therefore, if other lipidic substances such as squalene, cholesterol and wax esters, typical for the human sebum residue [30] are excluded, the sunflower oil appears to be an adequate substitute expected to show very similar chemical reactivity when performing various experiments based on interaction of this material with TBAI and NO_2 intended for study of the fingerprint's visualization mechanism.

In the first step TBAI-sunflower oil mixtures are prepared with low and high TBAI concentrations, labeled as Sample 2 (diluted) and Sample 2* (concentrated). The FTIR spectrum of the diluted sample is practically identical as the one of pristine sunflower oil, however, the sample with higher concentration of TBAI, besides the typical features originating from the oil, shows additional features. These features resemble group of medium and weak bands in 880-1035 cm^{-1} that are characteristic for C–N+ stretching vibrations in the quaternary alkylammonium cation [33-34], that are also observable in the spectrum of pristine TBAI (Sample 5), recorded as a reference for comparison.

The next experiment encompasses treatment of pristine sunflower oil with NO_2 gas (Sample 3). A medium to strong band at ~1557 cm^{-1} appears in the FTIR spectrum of this sample, attributed to asymmetric stretching vibrational modes in nitro ($–NO_2$) group [35-37]. However, the weak to medium band attributed to symmetric stretching in the $–NO_2$ group, expected to appear at

1389–1259 cm^{-1} [35], in the FTIR spectrum of Sample 3, is hardly resolvable due to interference with the bands arising from twisting and wagging $–CH_2–$ groups in long hydrocarbon chains in a similar wavenumber range [35]. Such bands from twisting and wagging $–CH_2–$ groups also appear in all spectra of Samples 0-2*, yet they are very weak in the case of human sebum residue (Sample 0). The identification of nitro groups in the spectrum of Sample 3 is suggesting that NO_2 gas is reacting with the sunflower oil (nitration). Similar chemical behavior is expected between NO_2 and the fingerprint sebaceous residue, possibly via complex mechanisms including addition of nitro group on a double bond in unsaturated fatty acids and their esters, and processes of hydrogen abstraction, alongside with double bond position rearrangements [37-40]. The band at ~1649 cm^{-1} in the spectrum of Sample 3 could be associated to C=C double bonds vibrations [27], presuming that either the nitration is not complete or processes of double bond position rearrangements indeed occur. However, as discussed above, this band can also be attributed to H–O–H bending vibrations in water molecules [29], and since a weak band, possibly arising from O–H stretching modes is observable at ~3470 cm^{-1}, this claim is reasonably strong. At this point the deconvolution between the bands originating from C=C double bond stretching and H–O–H bending vibrations is hardly possible, however vegetable oils, such as the sunflower oil, indeed contain significant amounts of unsaturated fatty acids, such as oleic and linoleic acid, and their esters [32], thus the presence of C=C double bonds cannot be simply excluded. Regardless of the possible water presence in Sample 3, the nitration reactions can be considered as concurrent with the set of reactions between NO_2 and the I^- anion from TBAI (Eq. 2–7) forming I_2 that further reacts with excess TBAI to form $TBAI_3$ (Eq. 1), as discussed above in this research, thus leading to varieties in the color of the visualized fingerprints (see Figure 1).

In the final experiment, low and high amount of TBAI was mixed with sunflower oil, and these mixtures were exposed to NO_2 gas. The samples are abbreviated as Sample 4 for lower- and Sample 4* for higher TBAI concentration, respectively (see Table S4 in the SI). The spectrum of Sample 4 resembles all features as the case of Sample 3 - spectrum, however the band attributed to the asymmetric stretching vibrations in nitro group at ~1556 cm^{-1} [35-37] is significantly weaker. Similar weaker nitro group band compared to the spectrum of Sample 3, can be observed in the case of Sample 4* with higher concentration of TBAI, however in the spectrum of the latter sample, besides the typical for Sample 3, additional features associated to the TBA^+ cation can be also observed, when compared to the reference spectrum of pristine TBAI (Sample 5). The diminishing of the nitro group bands in Samples 4 and 4* compared to Sample 3 is suggesting that the nitration processes

are less favorable than the reaction between TBAI and NO_2 (described with Eq. 2–7) leading to formation of $TBAI_3$ (Eq. 1) which, again, could be related to the yellow to brown color variations of the fingerprints during the visualization process, as presented in Figure S5. It appears that shorter exposure of the TBAI dusted latent fingerprint to NO_2 gas leads to development of light color (yellow or dark yellow), while longer NO_2 treatment (20 s or more), but this is not always the case. Namely, the NO_2 treatment duration in the case of the visualized fingerprints on paper, presented in Figure 1a, b, is equal (5 seconds) but the fingerprint on Figure 1b is dark brown, while on Figure 1a - orange with some dark brown spots. From this it can be actually assumed that it is not the NO_2 exposure duration that defines the color outcome during the visualization process, but rather the TBAI powder coverage during the dusting pre-treatment. It is important to note that, if latent fingerprint, is treated with NO_2 gas from 5 s up to 10 minutes, without pre-dusting with TBAI, no visualization occurs, as presented in Figure S6 in SI, and this is the justification why the NO_2 method, originally developed for visualization of latent fingerprints on thermal paper [13], was modified by introducing TBAI pre-treatment. This is suggesting that TBAI most probably plays additional role and that is phase-transfer catalyst that facilitates the delivery of NO_2 from the gaseous phase into the sebaceous residue. The nitration of sunflower oil in the absence of TBAI (Sample 3 – see Table S4 in SI) is possible but it requires vigorous and repetitive mixing of the oil with NO_2. Anyhow, recalling the results from the Raman spectroscopy characterization (Figure 2a) discussed above, the I_3^- anion from $TBAI_3$ is identified on the surface of all visualized fingerprints, regardless of the color appearance and the type of surface on which the fingerprints were impressed (Table S1 in SI), yet this technique is not sensitive enough in the configuration we used to identify the lipidic compounds (including nitro- fatty acids and their esters), possibly because of their amorphous nature. On the other hand, Raman spectroscopy appears to be significantly more useful to identify the formation of $TBAI_3$ from reaction between TBAI and NO_2, while the FTIR spectrum of the reaction product between TBAI and NO_2 (Sample 6) does not provide very significant identification information in terms of the stretching vibrational modes of triiodide anion which are low frequency and expected to appear at wavenumbers in the far-infrared region ~200 cm^{-1} [29]. Though, the typical features originating from the TBA^+ cation, that also appear in the spectrum of pristine TBAI, are identifiable: C–H stretching from butyl groups at 3000–2850 cm^{-1} [35]; weak band at ~1465 cm^{-1} that correspond to CH_2 groups scissoring modes [35]; very weak bands from twisting and wagging $–CH_2–$ groups (1330 and 1152 cm^{-1}) and medium band associated to symmetrical C–H bending modes in CH_3 groups at ~1379 cm^{-1} [35]; bending weak broad bands at 1035–880 cm^{-1} that are characteristic for quaternary

alkylammonium cation C–N+ stretching- [33-34] and rocking-bending vibrations in $–CH_2–$ groups at ~730 cm^{-1} [35]. The band at ~1635 cm^{-1} is suggesting H–O–H bending vibrations in water molecules [29], even though the expected bands above 3000 cm^{-1} for O–H stretching vibrational modes [29], are not identifiable, possibly due to presence of only trace amounts of water.

Characterization with ^{1}H NMR spectroscopy

The last discussion in this research is dedicated to the results from characterization with ^{1}H NMR spectroscopy. The ^{1}H NMR instrumental setup and parameters are presented in the Supplementary Information - SI (sample preparation is described in Table S5). The characteristic features as chemical shift positions are presented in Table S6 and the spectra for all samples, in Figures S7–S12 in SI. Starting with assignation of the features in ^{1}H NMR spectrum of pristine sunflower oil Sample 1 - (Table 2 in the main text and Figure S7a–c in SI), aliphatic peaks (0.75–1.51 ppm) confirm the presence of long hydrocarbon chains involving protons from $–CH_2–$ and terminal $–CH_3$ groups in fatty acids and their esters [32, 41]. The peaks at 1.89–2.73 ppm can be assigned to $–CH_2–$ protons from allyl and double allyl groups typical for oleic and linoleic acids and their esters in sunflower oil, and $–CH_2–$ protons bound to ester groups [32, 41]. Protons originating from glycerol backbone in the fatty acid esters typically appear at 3.96–5.24 ppm, while the peaks at 5.29–5.34 ppm can be assigned to protons in –CH=CH– groups [32, 41] again typical for unsaturated fatty acids and their esters, even though, as discussed in the previous subsection dedicated to FTIR characterization, it was difficult to deconvolute the band associated with C=C stretching from the one originating from H–O–H bending vibrational modes.

When TBAI is mixed with sunflower oil (Sample 2), besides the ^{1}H NMR features associated to the sunflower oil itself, discussed above, the spectra (Table S6 and Figure S8a–d in SI) show additional features originating from TBAI that are also identifiable in the spectra of pristine dry TBAI reference sample (Sample 5, Figure S11a, b in SI). Namely, the $–CH_3$ and $–CH_2–$ protons from the *n*-butyl groups in TBAI appear significantly downfield compared to the protons from the hydrocarbon chains in various fatty acids and their esters present in the sunflower oil, likely caused by strong de-shielding effect from the positively charged nitrogen atom and iodide anion. The chemical shift intervals 0.92–0.95 ppm, 1.28–1.36 ppm, 1.54–1.58 ppm and 3.15–3.18 ppm can, most probably, be assigned to protons from terminal $–CH_3$ group, from $–CH_2–$ group bound to terminal $–CH_3$, internal $–CH_2–$ group and $–CH_2–$ group bound to the positively charged nitrogen atom in TBA^+ cation, respectively [21].

The strong singlet peak at 3.31 ppm, also observable in Sample 4 and Sample 5, is possibly originating from water impurities [42].

Treating pristine sunflower oil with NO_2 gas, without- (Sample 3) and in the presence of TBAI (Sample 4), leads to formation of compounds that generally show de-shielding effect in the peak positions compared to the pristine oil as presented in Table S6 in SI and in Figure S9a–c and Figure S10a–d in SI, for Sample 3 and 4, respectively. Namely, it can be observed from the spectra and the values in Table S6 in SI that the protons from $–CH_3$, $–CH_2–$, the glycerol backbone and from –CH=CH– groups indeed show downfield chemical shift values in Sample 3 and 4 compared to Sample 1. According to some literature data [37], features from strongly de-shielded protons originating from $–CH=C–NO_2$, $–CH_2–CH=CH–$ and –CH=CH–CH= groups, at ~7.52, ~6.32 and ~6.19 ppm, respectively, as product from nitration of linoleic acid, are also expected to appear at in the spectrum, however they are not observable in Figure S9a–9c and S10a–d in SI. The identification of nitro group using FTIR characterization as band at ~1557 cm^{-1} arising from asymmetric stretching vibrations, discussed in the previous subsection, undoubtedly refers that nitro-fatty acids and their esters are being synthesized. Hence, the probable explanation for not observing the abovementioned ^1H NMR features (6.2–7.5 ppm) associated to highly de-shielded protons, could be lack of conjugations between the C=C double bonds and/or between C=C double bonds and nitro group in the reaction products. This is possibly suggesting that the nitration mechanism is either based on synthesis of unsaturated- but non-conjugated compounds via hydrogen abstraction that could also involve double-bond rearrangement mechanism, or saturated nitro-fatty acids and their esters via nitro group addition mechanism [37-40].

Finally, when pristine TBAI is treated with NO_2 gas (Sample 6), slight shielding effect of the protons in the *n*-butyl groups can be observed in the ^1H NMR spectra compared to pristine TBAI (Table S6 and Figure S12a, b vs. S11a, b in SI). The explanation for the upfield shift possibly is a consequence to formation of the I_3^- anion, i.e. $TBAI_3$, when the I^- anion from TBAI and I_2 react (Eq. 1). The I_3^- represents a linear anion with delocalized electronic structure, showing less tendency for electron attraction compared to the I^- anion, hence causing shielding effect in the four *n*-butyl groups protons. Furthermore, an interesting observation is present in the ^1H NMR spectra of Sample 6, that is a weak broad feature at 7.52 ppm. Features around that position are characteristic for strongly de-shielded aromatic protons [35], but in this case, such feature is possibly attributed to a proton that is directly interacting with the electronically delocalized I_3^- anion.

The process of latent fingerprints visualization and the most important findings from the systematic spectroscopic characterization combined with various control and validation experiments are depicted in Scheme 1.

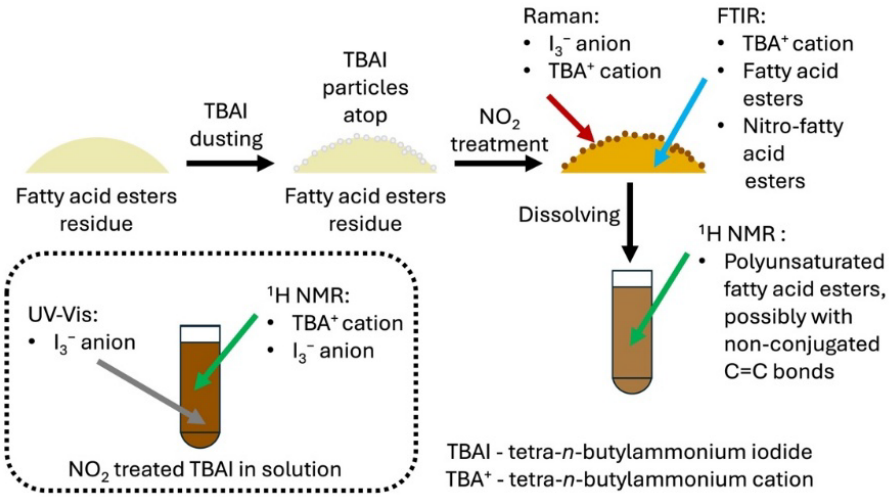

Scheme 1. Visualization of sebaceous latent fingerprints, characterization approach and results.

CONCLUSIONS

A two-step method intended for visualization of sebaceous latent fingerprints, on various porous and non-porous surfaces, is proposed in this research, based on tetra-*n*-butylammonium iodide (TBAI) dusting, followed by treatment with NO_2 gas (TBAI/NO_2 method).

The proposed method is simple, fast and reliable. It shows very significant identification capacity by reaching high number of second-level characteristics and additionally third-level features can be revealed.

The characterization with Raman spectroscopy identified I_3^- anion when TBAI pre-dusted fingerprints are treated with NO_2 gas and moreover identified both I_3^- anion and features associated to TBA^+ cation when TBAI powder is treated with NO_2 gas, suggesting formation of tetra-*n*-butylammonium triiodide – $TBAI_3$.

The UV-Vis spectroscopy characterization of the product, obtained from NO_2 treatment of TBAI, shows features that are characteristic for both I_3^- anion and molecular I_2, suggesting that both species are in equilibrium and the latter specie is formed via NO_2 caused oxidation of the I^- anion from

TBAI. I_2 further reacts with excess TBAI leading to formation of I_3^- anion i.e. $TBAI_3$. The molecular I_2 and the processes leading to its formation play the key role in the fingerprint's visualization mechanism, while $TBAI_3$ that resembles dark color, is providing the dominating contrast in the fingerprint's visualization process versus the substrates background surface.

The I_3^- is also identified on a fingerprint that was visualized two months prior to characterization, showing that the visualized fingerprints are composition-wise stable, making the proposed $TBAI/NO_2$ method very suitable for preserving forensic evidence.

FTIR and ^1H NMR spectroscopy characterization revealed that, even though the reaction between I_2 and excess TBAI, obtaining dark colored $TBAI_3$, is the main process leading to latent fingerprints visualization, the formation of nitro fatty acid esters, possibly with non-conjugated C=C bonds, caused by nitration of the lipidic residues, is also contributing towards the coloration effect considering that such nitro compounds appear orange-yellowish to brown in color.

The color outcome of the visualized fingerprints is mostly dependent on the TBAI coverage during the process of surface dusting and finally, besides a reactant, TBAI plays a role as a phase-transfer catalyst that allows NO_2 to penetrate into the bulk of fingerprint's sebaceous residue, thus subjecting this material to nitration reactions.

EXPERIMENTAL SECTION

The latent sebaceous fingerprints are deposited on various porous and non-porous surfaces (Table 1 and Table 2) using right hand forefinger after rubbing the forefinger near the nose. The visualization procedure encompasses two steps: Brush dusting of the latent fingerprints with powdered TBAI, followed by 5 seconds exposure to NO_2 gas (Figure 1 – visualized fingerprints). The NO_2 gas is generated by reaction between Zn pellets and 1:1 diluted HNO_3 [13]. After the visualization process, the fingerprints are subjected to forensic evaluation. The fingerprints, as well as the validation samples are characterized using spectroscopic methods (Raman, UV-Vis, FTIR and ^1H NMR spectroscopy). All details regarding the utilized reagents, methodology, validation experiments and characterization procedures can be found in the Supplementary Information – SI file.

Supplementary Information:

SI file is uploaded on zenodo.org and available at:
https://doi.org/10.5281/zenodo.19711846

ACKNOWLEDGMENTS

The authors are thankful to Mr. Manish Kumar of Sophisticated Analytical Instrumentation Facility (SAIF) Center, Panjab University, Chandigarh, India, for extending the facilities for NMR analysis.

REFERENCES

1. D. A. Crown, *J. Crim. L. & Criminology* **1969**, *60*, 258-264 https://scholarlycommons.law.northwestern.edu/jclc/vol60/iss2/17
2. O. P. J. M. I. U. A. Singla, *Identification Evidence* **2003** https://www.researchgate.net/profile/O-P-Jasuja/publication/372941076
3. W. J. Watling; K. O. Smith; *J. Forensic Identif.*, **1993**, *43*, 131-134 https://www.ojp.gov/ncjrs/virtual-library/abstracts/heptane-alternative-freonninhydrin-mixture
4. N. Meylan; C. J. Lennard; P. A. Margot; *Forensic Sci. Int.*, **1990**, *45*, 73-83 https://doi.org/10.1016/0379-0738(90)90223-L
5. P. F. Kelly; R. S. P. King; B. Shah; R. J. Mortimer; presented at *SPIE Security + Defence*, Berlin, Germany **2009** https://doi.org/10.1117/12.833980
6. B. C. Shah; *Doctor of Philosophy Doctoral Thesis*, *Loughborough University*, Loughborough, **2013** https://hdl.handle.net/2134/12533
7. K. T. Clarke; S. L. Cresswell; W. J. Gee; *Analyst* **2023**, *148*, 5547-5563 http://dx.doi.org/10.1039/D3AN01112G
8. S. M. Bleay; M. J. Bailey; R. S. Croxton; S. Francese; *WIREs Forensic Science*, **2021**, *3*, e1403 https://doi.org/10.1002/wfs2.1403
9. O. P. Jasuja; A. Kaur; P. Kumar; *Forensic Sci. Int.*, **2012**, *223*, e47-e52 https://doi.org/10.1016/j.forsciint.2012.09.013
10. K. Kumari Sharma; G. H. Kannikanti; T. R. R. Baggi; J. R. Vaidya; *J. Forensic Sci.*, **2019**, *64*, 1859-1866 https://doi.org/10.1111/1556-4029.14139
11. V. Singh; P. Mandal; S. Stojkovikj; M. Najdoski; O. Slobodan; O. P. Jasuja; *J. Indian Chem. Soc*.,**2025**, *102*, 101694 https://doi.org/10.1016/j.jics.2025.101694
12. M. J. Baker; J. Trevisan; P. Bassan; R. Bhargava; H. J. Butler; K. M. Dorling; P. R. Fielden; S. W. Fogarty; N. J. Fullwood; K. A. Heys; C. Hughes; P. Lasch; P. L. Martin-Hirsch; B. Obinaju; G. D. Sockalingum; J. Sulé-Suso; R. J. Strong; M. J. Walsh; B. R. Wood; P. Gardner; F. L. Martin; *Nat. Protoc*., **2014**, *9*, 1771-1791 https://doi.org/10.1038/nprot.2014.110
13. S. Stojkovikj; S. Oklevski; O. P. Jasuja; M. Najdoski; *Forensic Chem*., **2020**, *17*, 100196 https://doi.org/10.1016/j.forc.2019.100196
14. B. T. Ulery; R. A. Hicklin; G. I. Kiebuzinski; M. A. Roberts; J. Buscaglia; *Forensic Sci. Int*., **2013**, *230*, 99-106 https://doi.org/10.1016/j.forsciint.2013.01.012
15. M. K. Thakar; T. Sharma; *Egypt. J. Forensic Sci*., **2016**, *6*, 194-201 https://doi.org/10.1016/j.ejfs.2016.05.008

16. L. Andrews; E. S. Prochaska; A. Loewenschuss; *Inorg. Chem.*, **1980**, *19*, 463-465 https://doi.org/10.1021/ic50204a036
17. J. C. Rubim; O. Sala; *J. Raman Spectrosc.*, **1981**, *11*, 320-321 https://doi.org/10.1002/jrs.1250110505
18. P. H. Svensson; L. Kloo; *J. Chem. Soc., Dalton Trans.*, **2000**, 2449–2455 https://doi.org/10.1039/B002492I
19. A. J. Blake; C. Castellano; V. Lippolis; E. Podda; M. Schröder; *Acta Crystallogr. C*., **2024**, *80*, 311-318 https://doi.org/10.1107/S2053229624004194
20. Y. Jin; M. Kida; J. Nagao; *J. Chem. Eng. Data*, **2016**, *61*, 679-685 https://doi.org/10.1021/acs.jced.5b00842
21. R. Chromá; M. Vilková; I. Shepa; P. Makoś-Chełstowska; V. Andruch; *J. Mol. Liq*., **2021**, *330*, 115617 https://doi.org/10.1016/j.molliq.2021.115617
22. N. Hattori; M. Hara; H. Okabayashi; C. J. O'Connor; *Colloid Polym. Sci*., **1999**, *277*, 306-317 https://doi.org/10.1007/s003960050386
23. Y. Miwa; T. Nagahama; H. Sato; A. Tani; K. Takeya; *Molecules* **2022**, *27*. https://doi.org/10.3390/molecules27154743
24. E. O'Neill; R. Z. Hinrichs; Journal of Geophysical Research: *Atmospheres* **2011**, *116* https://doi.org/10.1029/2010JD014880
25. R. Xian; G. Corthey; D. M. Rogers; C. A. Morrison; V. I. Prokhorenko; S. A. Hayes; R. J. D. Miller; *Nat. Chem*., **2017**, *9*, 516-522 https://doi.org/10.1038/nchem.2751
26. J. M. Gardner; M. Abrahamsson; B. H. Farnum; G. J. Meyer; *J. Am. Chem. Soc*., **2009**, *131*, 16206-16214 https://doi.org/10.1021/ja905021c
27. K. D. Mekonnen; Heliyon **2023**, *9* https://doi.org/10.1016/j.heliyon.2023.e14699
28. A. S. Anderson; J. E. Fulton; *J. Investig. Dermatol*., **1973**, *60*, 115-120 https://doi.org/10.1111/1523-1747.ep12682018
29. K. Nakamoto, Infrared and raman Spectra of inorganic and coordination compounds. In *Handbook of Vibrational Spectroscopy*, E. J. M. Chalmers., P. R. Griffiths Eds.; John Wiley & Sons, Ltd., New York, **2006**. https://doi.org/10.1002/0470027320.s4104
30. A. Girod; R. Ramotowski; C. Weyermann; *Forensic Sci. Int*., **2012**, *223*, 10-24 https://doi.org/10.1016/j.forsciint.2012.05.018
31. A. Pappas; J. Fantasia; T. Chen; *Dermatoendocrinol.*, **2013**, *5*, 319-324 https://doi.org/10.4161/derm.25366
32. P. P. Chiplunkar; A. P. Pratap; *Prog. Org. Coat*., **2016**, *93*, 61-67 https://doi.org/10.1016/j.porgcoat.2016.01.002
33. A. S. Hume; W. C. Holland; F. Fry; *Spectrochim. Acta A Mol. Biomol. Spectrosc*., **1968**, *24*, 786-788 https://doi.org/10.1016/0584-8539(68)80109-6
34. N. Zaltsman; D. Kesler-Shvero; E. I. Weiss; N. Beyth; *J. Appl. Biomater. Funct. Mater.*, **2016**, *14*, 205-211 https://doi.org/10.5301/jabfm.5000269
35. R. M. Silverstein; F. X. Webster; D. Kiemle; *Spectrometric Identification of Organic Compounds*, 7th Edition, John Wiley & Sons, New York, **2005**
36. M. Hassan; S.-C. Krieg; C. Ndefo Nde; J. Roos; T. J. Maier; E. A. El Rady; M. A. Raslan; K. U. Sadek; G. Manolikakes; *Eur. J. Org. Chem.*, **2021**, *2021*, 2239-2252 https://doi.org/10.1002/ejoc.202100247

37. M. Fazzari; S. R. Woodcock; P. Rowart; K. Ricart; J. R. Lancaster; R. Patel; D. A. Vitturi; B. A. Freeman; F. J. Schopfer; *Redox Biol.*, **2021**, *41*, 101913 https://doi.org/10.1016/j.redox.2021.101913
38. S. R. Woodcock; G. Bonacci; S. L. Gelhaus; F. J. Schopfer; *Free Radic. Biol. Med.*, **2013**, *59*, 14-26 https://doi.org/10.1016/j.freeradbiomed.2012.11.015
39. V. B. O'Donnell; J. P. Eiserich; P. H. Chumley; M. J. Jablonsky; N. R. Krishna; M. Kirk; S. Barnes; V. M. Darley-Usmar; B. A. Freeman; *Chem. Res. Toxicol.*, **1999**, *12*, 83-92. https://doi.org/10.1021/tx980207u
40. W. A. Pryor; J. W. Lightsey; D. F. Church; *J. Am. Chem. Soc.*, **1982**, *104*, 6685-6692 https://doi.org/10.1021/ja00388a035
41. S. D. Caño-Ochoa; A. Ruiz-Aracama; M. D. Guillén; *Antioxidants*, **2022**, *11*, 722 https://doi.org/10.3390/antiox11040722
42. G. R. Fulmer; A. J. M. Miller; N. H. Sherden; H. E. Gottlieb; A. Nudelman; B. M. Stoltz; J. E. Bercaw; K. I. Goldberg; *Organometallics*, **2010**, *29*, 2176-2179 https://doi.org/10.1021/om100106e